ISSN 1674-1056
http://cpb.iphy.ac.cn
http://iopscience.iop.org/cpb
中国物理 B
Chinese Physics
中国物理 Chinese Physics B

First-principles study of high performance lithium/sodium storage of $Ti_3C_2T_2$ nanosheets as electrode materials

Li-Na Bai(白丽娜)[1], Ling-Ying Kong(孔令莹)[1], Jing Wen(温静)[1], Ning Ma(马宁)[2], Hong Gao(高红)[1], Xi-Tian Zhang(张喜田)[1,3]

Citation: Chin. Phys. B . 2020, 29(1): 016802 . **doi:** 10.1088/1674-1056/ab592e
Journal homepage: http://cpb.iphy.ac.cn; http://iopscience.iop.org/cpb

What follows is a list of articles you may be interested in

Real-space observation on standing configurations of phenylacetylene on Cu (111) by scanning probe microscopy

Jing Qi(戚竞), Yi-Xuan Gao(高艺璇), Li Huang(黄立), Xiao Lin(林晓), Jia-Jia Dong(董佳家), Shi-Xuan Du(杜世萱), Hong-Jun Gao(高鸿钧)

Chin. Phys. B . 2019, 28(6): 066801 . **doi:** 10.1088/1674-1056/28/6/066801

Interaction of two symmetric monovacancy defects in graphene

Wen-Yan Xu(徐文焱), Li-Zhi Zhang(张礼智), Li Huang(黄立), Yan-De Que(阙炎德), Ye-Liang Wang(王业亮), Xiao Lin(林晓), Shi-Xuan Du(杜世萱)

Chin. Phys. B . 2019, 28(4): 046801 . **doi:** 10.1088/1674-1056/28/4/046801

Domain boundaries in silicene: Density functional theory calculations on electronic properties

Xiao Hong-Jun, Zhang Li-Zhi, Du Shi-Xuan, Gao Hong-Jun

Chin. Phys. B . 2015, 24(8): 086806 . **doi:** 10.1088/1674-1056/24/8/086806

Adsorption of glycine on diamond (001): Role of bond angle ofcarbon atoms

Li Lin, Xu Jing, Xu Li-Fang, Lian Chao-Sheng, Li Jun-Jie, Wang Jian-Tao, Gu Chang-Zhi

Chin. Phys. B . 2015, 24(5): 056803 . **doi:** 10.1088/1674-1056/24/5/056803

First-principles study of Ar adsorptions on the (111) surfaces of Pd, Pt, Cu, and Rh

Niu Wen-Xia, Zhang Hong, Gong Min, Cheng Xin-Lu

Chin. Phys. B . 2013, 22(6): 066802 . **doi:** 10.1088/1674-1056/22/6/066802

First-principles study of high performance lithium/sodium storage of $Ti_3C_2T_2$ nanosheets as electrode materials*

Li-Na Bai(白丽娜)[1], Ling-Ying Kong(孔令莹)[1], Jing Wen(温静)[1], Ning Ma(马宁)[2], Hong Gao(高红)[1], and Xi-Tian Zhang(张喜田)[1,3,†]

[1] *Key Laboratory for Photonic and Electronic Bandgap Materials, Ministry of Education, School of Physics and Electronic Engineering, Harbin Normal University, Harbin* 150025, *China*

[2] *School of Computer Science and Information Engineering, Harbin Normal University, Harbin* 150025, *China*

[3] *Department of Physics, Harbin Institute of Technology, Harbin* 150001, *China*

(Received 2 September 2019; revised manuscript received 14 November 2019; accepted manuscript online 20 November 2019)

$Ti_3C_2T_x$ nanosheet, the first synthesized MXene with high capacity performance and charge/discharge rate, has attracted increasingly attention in renewable energy storage applications. By performing systematic density functional theory calculations, the theoretical capacity of the intrinsic structure of single- and multi-layered $Ti_3C_2T_2$ (T = F or O) corresponding to M (M = Li and Na) atoms are investigated. Theoretical volumetric capacity and gravimetric capacity are obtained, which are related to the stacking degree. The optimal ratios of capacity to structure are determined under different stacking degrees for understanding the influence of surface functional groups on energy storage performance. Its performance can be tuned by performing surface modification and increasing the interlayer distance. In addition, the reason for theoretical capacity differences of M atoms is analyzed, which is attributed to difference in interaction between the M-ions and substrate and the difference in electrostatic exclusion between adsorbed M-ions. These results provide an insight into the understanding of the method of efficiently increasing the energy storage performance, which will be useful for designing and using high performance electrode materials.

Keywords: density functional theory, MXene, electrode materials

PACS: 68.35.Md, 68.43.–h, 68.43.Fg **DOI:** 10.1088/1674-1056/ab592e

1. Introduction

Efficient electrical energy storage devices (EES) are urgently needed for the efficient use of renewables, including wind, solar, and tidal energy, *etc*. Among different EES devices, rechargeable batteries, such as Li ion batteries (LIBs) and Na ion batteries (NIBs), are considered to be promising devices to store the energy.[1] However, the performance of ion batteries can hardly satisfy the growing demand for large-scale energy storage. It is noteworthy that the performance of ion batteries is highly dependent on the properties of electrode materials. For electrode material, the energy storage involves physical interaction and/or chemical reaction at the surface or interface. Consequently, a promising strategy to create high energy storage ion batteries is to develop new electrode material with large specific surface area and high electrical conductivity.

Two-dimensional (2D) materials have shown great promise in electrode material applications due to the large specific surface area, tunable electronic properties, and extraordinary mechanical strength.[2] For instance, graphene and its oxide,[3–6] exfoliated nanosheets of metal–organic frameworks (MOFs),[7] phosphorene,[8] and layered molybdenum disulphide (MoS_2)[9] have already shown promising results as electrode materials. Recently, 2D transition metal carbides/carbonitrides (denoted as MXenes) have attracted significant attention as electrode materials.[10–15] MXene can be prepared from the early ternary transition metal carbides, nitrides, or carbonitrides (*MAX*) by means of the etching approaches, where M is an early transition metal (M = Sc, Ti, V, Cr, Zr, Nb, Mo, Hf, Ta, W), A is mainly a group IIIA or IVA element (A = Al, Si, Ga, Ge, In, Sn), X is C or/and N, and n = 1, 2 or 3.[16] In the exfoliation process, the A atoms are replaced by T-terminations (T = F, O or OH), leading to functionalized MXene.[17–19]

Among MXenes, $Ti_3C_2T_x$ is considered as the most promising candidate for electrode material.[20–22] Many theoretical[23–29] and experimental[30–33] researches of energy storage properties, and influence of some terminal groups for storage properties, *etc*. have been well carried out from pure science to potential applications, However, the volumetric capacity of $Ti_3C_2T_x$ nanosheet corresponding to the intrinsic structure is still unclear. The finding optimal ratio of capacity to structure of Li/Na atom intercalation for Ti_3C_2-based 2D material is urgently needed to explain the limit of storage capacity for synthesizing $Ti_3C_2T_x$.

In this paper, the optimal capacity of Li/Na atom intercalation into Ti_3C_2 single- and multi-layers as well as its fluorinated and oxidized derivatives ($Ti_3C_2T_2$, T = F or O) are

*Project supported by the National Natural Science Foundation of China (Grant Nos. 51772069 and 51772070).

†Corresponding author. E-mail: xtzhangzhang@hotmail.com

© 2020 Chinese Physical Society and IOP Publishing Ltd

theoretically studied in detail based on first-principles calculations. We demonstrate that the energy storage performance can be tuned by performing the surface modification and increasing the interlayer distance. The $Ti_3C_2T_x$ nanosheets with an optimal volume-to-capacity ratio that will be helpful in increasing the volumetric capacity, are prepared. In addition, the energy cost at zero temperature and electron distribution are analyzed, which reasonably explains the fact that the theoretical capacity of Na atoms is lower than that of Li atoms on $Ti_3C_2T_2$ nanosheets.

2. Computational details

The calculations were performed by using the CASTEP code which is based on density functional theory through the ultrasoft pseudopotentials method.[34] The generalized gradient approximation including van der Waals dispersion corrections (DFT+D2) was used to optimize the geometric structure.[35,36] The plane wave energy cutoff was 340 eV for geometric optimization and 500 eV for electronic structure computation. Integration in the Brillouin zone was performed by using a k-point of $5\times5\times1$ mesh parameter grid for Ti_3C_2 and $Ti_3C_2T_2$ supercell. The spin-polarized calculations are conducted. To minimize systematic errors, the $2\times2\times1$ supercell of Ti_3C_2 and $Ti_3C_2T_2$ systems is used in all the following computations as shown in Fig. 1. The Ti_3C_2 and $Ti_3C_2T_2$ monolayers are represented by a vacuum width of 20 Å to avoid any interactions between the layered hexagonal structures and its periodically repeated images along the non-periodic direction (c axis). The Ti_3C_2 and $Ti_3C_2T_2$ nanosheets are constructed by adjusting the vacuum width along the c axis.

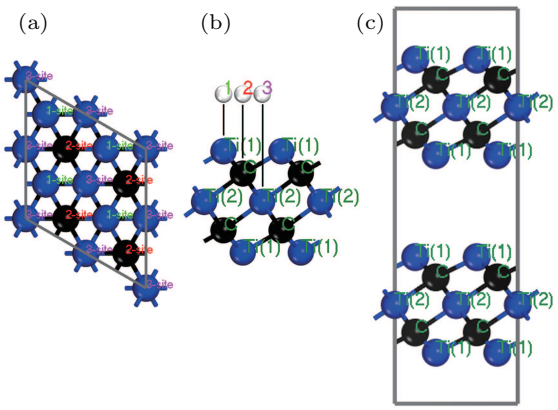


Fig. 1. Schematic diagram of crystal structure of $2\times2\times1$ supercell of Ti_3C_2 monolayer, showing (a) top view and (b) side view, and (c) $2\times2\times1$ supercell of Ti_3C_2 nanosheet. The monolayer is stacked in a sequence of Ti(1)–C–Ti(2)–C–Ti(1) to form the layered hexagonal structure of non-periodic, and the nanosheet of periodic structure is constructed by two layered hexagonal structures.

The formation energy (E_{form}) of $Ti_3C_2T_2$ monolayer is calculated by using the following formula

$$E_{\text{form}} = E_{\text{tot}}(Ti_3C_2T_2) - (1/2)E_{\text{tot}}(Ti_3AlC_2) + E_{\text{atom}}(Al) - 2E_{\text{atom}}(T_2), \quad (1)$$

where $E_{\text{tot}}(Ti_3C_2T_2)$ and $E_{\text{tot}}(Ti_3AlC_2)$ are the total energy of $Ti_3C_2T_2$ single layer and Ti_3AlC_2 unit cell, respectively, and E_{atom} is the energy of per atom in their corresponding bulk structure or molecule.

The adsorption energy (E_{ads1}) of one atom on the $Ti_3C_2T_2$ monolayer can be obtained from

$$E_{\text{ads1}} = E_{\text{adatom@system}} - E_{\text{system}} - E_{\text{atom}}. \quad (2)$$

The adsorption energy (E_{ads2}) of the multilayer atom on the $Ti_3C_2T_2$ monosheet is defined as

$$E_{\text{ads2}} = E_{\text{multilayers@system}} - E_{(y-1)\text{multilayers@system}} - 8E_{\text{atom}}, \quad (3)$$

where $E_{\text{adatom@system}}$ and E_{system} are, respectively, the total energy of single metal atom adsorbed and unadsorbed monolayer, $E_{\text{multilayers@system}}$ and $E_{(y-1)\text{multilayers@system}}$ are, respectively, the total energy of intercalation $2y$ and $2(y-1)$ layers' metal atom on both surfaces of single layer, E_{atom} is the energy of per metal atom from the bulk metal, and y represents the number of intercalation layers on each surface of single layer. When only one layer atom ($y=1$) is intercalated into each surface, the $E_{(y-1)\text{multilayers@system}}$ is the total energy of $Ti_3C_2T_2$ single layer.

The theoretical volumetric capacity (C_{VM}, in units $\text{mAh}\cdot\text{cm}^{-3}$) and the gravimetric capacity (C_{MM}, in units $\text{mAh}\cdot\text{g}^{-1}$) can be identified from the following calculation formula

$$C_{\text{VM}} = \frac{4(y\times z\times F\times 10^3)}{V_{\text{cell}}\cdot N_{\text{A}}}, \quad (4)$$

$$C_{\text{MM}} = \frac{2(y\times z\times F\times 10^3)}{M_{\text{mol}}}, \quad (5)$$

where z is the valence number ($z=1$ for Li and Na), F is the Faraday constant (26.81 $\text{Ah}\cdot\text{mol}^{-1}$), N_{A} is the Avogadro constant, V_{cell} represents the optimized cell volume of nanosheet, M_{mol} is the molar mass which includes the mass of the adsorbed M atoms, V_{cell} is defined as $V_{\text{cell}} = (\sqrt{3}/2)a^2c$, with a ($a=3.07$ Å) being the lattice constant of nanosheet and c being the lattice constant along the c-axis direction and is changed by adjusting the width of the vacuum inserted between two layered hexagonal structures. The coefficient $4\times y$ in formula (4) represents the total number of intercalation layers in the interlayer spacing of nanosheet, and the coefficient $2\times y$ in formula (5) represents the total number of intercalation layers on both surfaces of single layer. The reason for the difference between calculated coefficients from the two formulas is that the value of C_{MM} is determined by the molar mass of one layered hexagonal structure and the number of

adsorbed atoms on its upper and lower surface, and independent of crystal volume, while the value of C_{VM} is related to the crystal volume and the total number of atoms intercalated into the lattice, thus it is calculated by using a crystal structure that is composed of two layered hexagonal structures.

3. Results and discussion

3.1. Structure and stability of Ti_3C_2 and $Ti_3C_2T_2$ monolayers

As mentioned above, Ti_3C_2 can be prepared from the Ti_3AlC_2 by means of etching. The as-synthesized Ti_3C_2 has the fairly complex surface morphology with the mixed terminal groups (F, O, and OH) occurring.[37] The hydroxylated derivative is not included in our computations because the H atoms are relatively easy to replace.[17,38,39] The surface functionalizations of oxygen and fluoride are focused. The surface morphology of $Ti_3C_2T_2$ (T = F or O) has previously shown that MXene with complete and symmetrical surface terminations is more thermodynamically stable than those with partial and asymmetric surface terminations.[17,25,40] Therefore, three possible configurations of $Ti_3C_2T_2$ monolayer are constructed by saturating the dangling bond of surface Ti(1) atoms. In more detail, the T-terminations are equally and homogeneously distributed on both surfaces of monolayers, corresponding to the top position on Ti(1) atoms (1-top site), the hollow position on C atoms (2-hollow site), and the hollow position on Ti(2) atoms (3-hollow site) as shown in Fig. 1.

We start with considering structural optimizations to characterize the crystal structures of monolayers by using two methods, including the cases with and without van der Waals dispersion corrections. The structural information and calculated E_{form} are listed in Table 1. The calculated value of E_{form} is sensitive to the van der Waals dispersion correction. For the same $Ti_3C_2T_2$ configuration, the calculated E_{form} by the DFT+D2 method is 1 eV higher than that by the DFT method. However, it is found that the ground state configuration with van der Waals dispersion correction is similar to that without van der Waals dispersion correction, the T-terminations preferentially bind to the 3-hollow sites, which is also in agreement with the previous theoretical result.[23,25,28] This is because structural characteristics of $Ti_3C_2T_2$ single layer determine the sites that the terminations prefer to occupy. The Ti atoms tend to form six-fold coordination in this structure, thus the Ti-centered distorted octahedral structure of surfaces is constructed through T-terminations occupying the 3-sites.[41] The trends of energy variation after surface functionalization obtained by the two methods are also consistent with each other. The calculated E_{form} of Ti_3C_2 monolayer is obviously larger than that of the functionalized derivative. The positive value of E_{form} indicates that the Ti_3C_2 monolayer is difficult to form spontaneously through the selective etching of Al layers. On the contrary, the negative value of E_{form} shows that the $Ti_3C_2T_2$ monolayers obtained by the selective etching of the Ti_3AlC_2 phase are stable. Actually, the Ti_3C_2 monolayer without surface terminations has not yet been synthesized, and the presence of surface terminations conduces to the formation of monolayer.

Table 1. Optimized structural data (in unit Å) and calculated E_{form} values (in unit eV) of Ti_3C_2, $Ti_3C_2F_2$, and $Ti_3C_2O_2$ monolayers.

System	t	Bond lengths		E_{form}
	DFT/DFT+D2	DFT/DFT+D2		DFT/DFT+D2
		Ti(1)–C	Ti(2)–C	
Ti_3C_2	4.62/4.72	2.04/2.05	2.19/2.20	2.87/3.86
$Ti_3C_2F_2$-1 site	4.67/4.72	2.06/2.06	2.20/2.20	−6.23/−5.22
$Ti_3C_2F_2$-2 site	4.79/4.85	2.11/2.12	2.17/2.18	−7.15/−6.14
$Ti_3C_2F_2$-3 site	4.66/4.70	2.06/2.07	2.18/2.19	−8.03/−6.93
$Ti_3C_2O_2$-1 site	4.94/4.96	2.13/2.14	2.19/2.19	−1.84/−1.19
$Ti_3C_2O_2$-2 site	5.10/5.13	2.24/2.24	2.13/2.13	−5.68/−4.89
$Ti_3C_2O_2$-3 site	5.14/5.17	2.21/2.21	2.17/2.18	−7.28/−6.38

The structural properties of ground state of Ti_3C_2 and $Ti_3C_2T_2$ monolayer are investigated. The t is defined as the vertical distance between the top Ti(1) atom and bottom Ti(1) atom. Based on our structural models, the difference between structure properties obtained by using DFT and DFT+D2 methods is limited to 0.5%. Therefore, the optimized structure of monolayer is not very sensitive to the van der Waals dispersion correction. Compared with the Ti_3C_2 monolayer, the T-terminated Ti_3C_2 monolayer has larger calculated t and the surface Ti(1)–C bond length, implying that surface terminations strongly interact with the original Ti_3C_2 structure, which is consistent with previous theoretical result.[23,25]

3.2. Single M atom adsorption on surfaces of Ti_3C_2 and $Ti_3C_2T_2$ monolayers

After a thorough understanding of the structure properties of monolayers, we subsequently extend our computations to their adsorption behaviors of the single M (M = Li and Na) atom. Those adsorption configurations of one M atom on three possible adsorption sites of surfaces are considered (1-, 2-,

and 3-sites as shown in Fig. 1), corresponding to a chemical stoichiometric ratio for each of $Ti_3C_2M_{0.25}$ and $Ti_3C_2T_2M_{0.25}$. To quantitatively evaluate the adsorption behaviors, the calculated E_{ads1}, and optimal adsorption height (h) and Hirshfeld charge of the adsorbed atom are calculated by using the DFT and DFT+D2 methods. The h is defined as the vertical distance from the M atom to the surface layer of Ti(1) atom. The Hirshfeld charge is defined as being relative to the deformation density, this is the difference between atomic charge densities after and before relaxation. After full geometry relaxation, the relative stabilities of adsorption configurations can be determined through calculating the value of E_{ads1}.

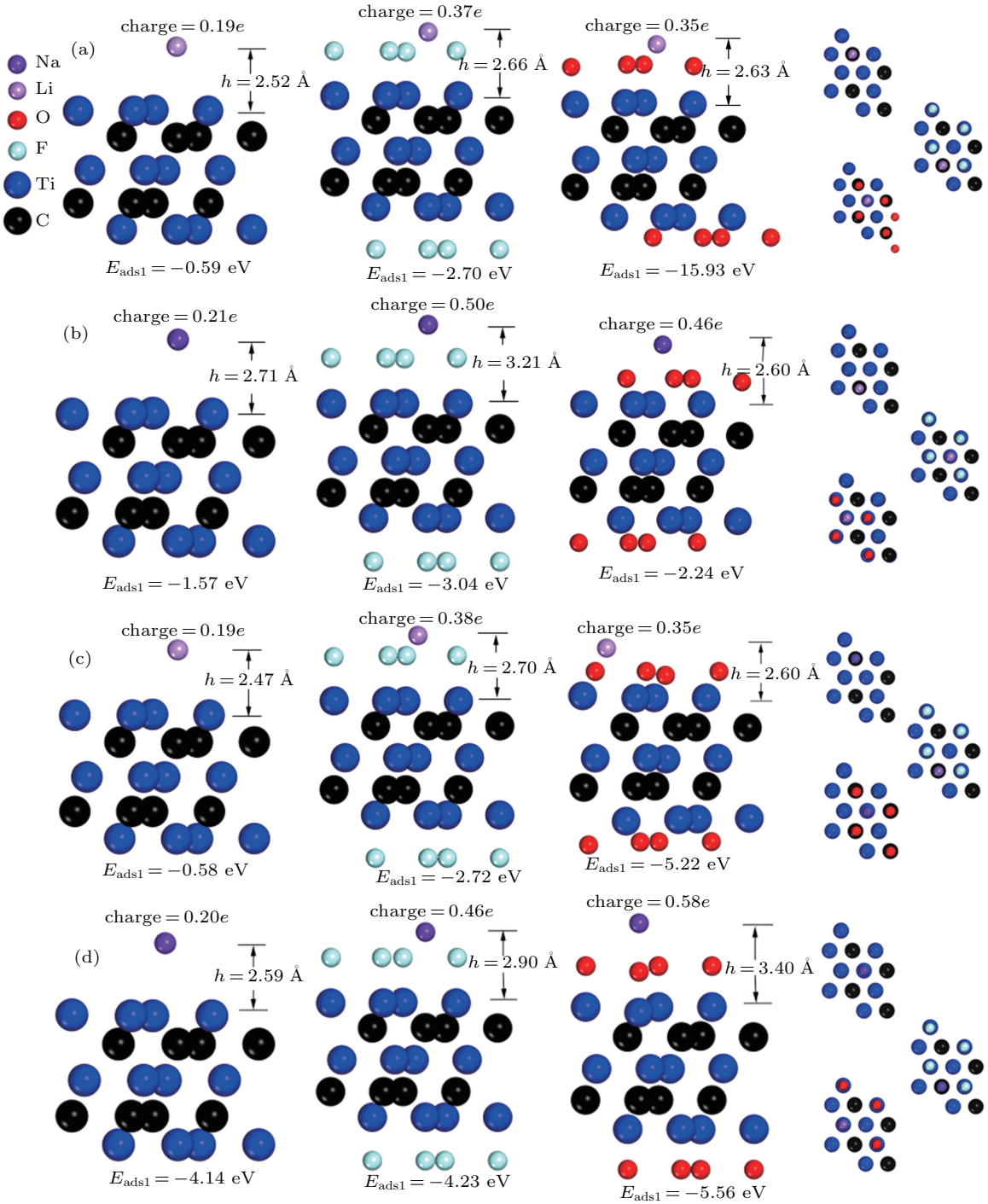


Fig. 2. The most stable adsorption configurations (side and top views) of (a) $Ti_3C_2Li_{0.25}$ and $Ti_3C_2T_2Li_{0.25}$ systems, (b) $Ti_3C_2Na_{0.25}$ and $Ti_3C_2T_2Na_{0.25}$ systems obtained by using DFT method, and (c) $Ti_3C_2Li_{0.25}$ and $Ti_3C_2T_2Li_{0.25}$ systems, (d) $Ti_3C_2Na_{0.25}$ and $Ti_3C_2T_2Na_{0.25}$ systems obtained by using DFT+D2 method with their calculated values of E_{ads1}, h, and Hirshfeld charge.

The most stable adsorption configurations with their calculated E_{ads1}, h, and Hirshfeld charge are shown in Fig. 2. For the $Ti_3C_2M_{0.25}$ configurations, the M atom prefers to sit at the hollow site due to repulsive interaction between the positively charged M and Ti atoms. When the functional groups exist, the M atom migrates to the nearest hollow site on the terminations that occupy the 1-top site, except the $Ti_3C_2O_2Na_{0.25}$ configuration obtained by using the DFT method. In previous

analysis of the ground state configuration of $Ti_3C_2T_2$ monolayers, the T-terminations preferentially bind to the 3-hollow sites. Therefore, the M atom tends to stay away from the site that the terminations most prefer to occupy within the monolayer. The relative structural stability of adsorption configuration depends mainly on the possible charge transfer between adsorbed atom and terminal atom. If adsorbed metal atoms can provide sufficient electrons for the terminal atoms, then the T-terminations occupying the 1-top sites become the most stable configuration of $Ti_3C_2T_2M_{0.25}$. Here it is clearly observed that the calculated E_{ads1} of $Ti_3C_2T_2$ monolayer with or without van der Waals dispersion corrections, is lower than that of Ti_3C_2 monolayer. Further, the calculated value of Hirshfeld charge for $Ti_3C_2T_2$ monolayer is higher than that of Ti_3C_2 monolayer. The low adsorption energy and the large charge transfer suggest that the M atom prefers to adsorb on the T-terminated Ti_3C_2 surface. This may relate to the strong interaction between functional group and metal atom.

3.3. Stable multilayer intercalation among M atoms in Ti_3C_2 and $Ti_3C_2T_2$ nanosheets

After a thorough understanding of the adsorption behaviors of one M atom on the surfaces, we check the variation of adatom concentration as a function of lattice parameters c. In this subsection, the multilayer incorporation of metal atom into nanosheets is focused by performing the DFT method. To check the possible multilayer incorporation, the quasi-symmetrically adsorption configurations are used, corresponding to the chemical stoichiometric ratio of $Ti_3C_2M_{2y}$ and $Ti_3C_2T_2M_{2y}$. Here, three different incorporation atom concentrations ($y = 1$–3) are considered. Since M atoms' orderings can be different for the same incorporation concentration, the geometry optimization is performed for all possible structures, here more than 100 structures are considered. To investigate the structural stabilities, the calculated E_{ads2} as a function of lattice constant c is analyzed. The energetically favorable structures with the same lattice constant are determined by comparing their relative E_{ads2}. The calculated E_{ads2} values of the most energetically favorable structures of different intercalation layers as a function of lattice constant c are shown in Fig. 3.

In Fig. 3, the calculated E_{ads2} of intercalating the same number of atomic layers into the interlayer spacing of nanosheet decreases gradually with the increase of lattice constant c. The critical value of lattice constant c of intercalating the same number of atomic layers is determined by obtaining the inflection points between the positive and negative values of adsorption energy, thus, the minimum lattice volume and the maximum volumetric capacity can be predicted in the bulk-stacking Ti_3C_2 and $Ti_3C_2T_2$ nanosheet with the determined number of M atomic layers. When each additional layer of M atoms is intercalated, the calculated E_{ads2} has a process of change from high energy to low energy with the increase of lattice constant c. For example, under the same lattice constant c ($c = 37.04$ Å), the calculated E_{ads2} value of $Ti_3C_2F_2Li_4$ nanosheet and that of $Ti_3C_2F_2Li_6$ nanosheet are greatly different from each other, which phenomenon is attributed to the increase of the Coulomb repulsive between the M atoms with the number of intercalated atoms increasing. With the increase of lattice constant c, the calculated E_{ads2} of $Ti_3C_2F_2Li_6$ nanosheet decreases gradually. Once calculated E_{ads2} is lower than zero, multilayer adsorption structure is stable, indicating that the interlayer spacing variation should affect the number of intercalating atomic layers, and the intercalation layer number increases with lattice constant c increasing. In the multilayers studied above, the distance from the bottom of one $Ti_3C_2T_x$ sheet to the top of the next sheet is around 5.0 Å,[20] indicating that the sheets are bound mainly by van der Waals interaction, and at most two layers' M atoms can be incorporated into the interlayer spacing between two layered hexagonal structures. As the lattice expands along the c-axis direction in a wide range, more metal atoms can be incorporated into the interlayer spacing. When the chemical stoichiometric ratio of M atom to Ti atom are larger than $2y/3$ ($y = 1$ or 2), some M atoms are driven to penetrate into the sub-adjacent region of the surface, resulting in the multilayer adsorption in the space region. A similar multilayer adsorption behavior has also been found in previous work.[26] Overall, the prepared $Ti_3C_2T_x$ monolayers and the expansion of the interlayer spacing of $Ti_3C_2T_x$ nanosheets will be helpful in increasing the number of incorporation atom layers. Actually, the interlayer-expanded Ti_3C_2 has been synthesized experimentally, and its Li storage capacity was improved.[31,42,43]

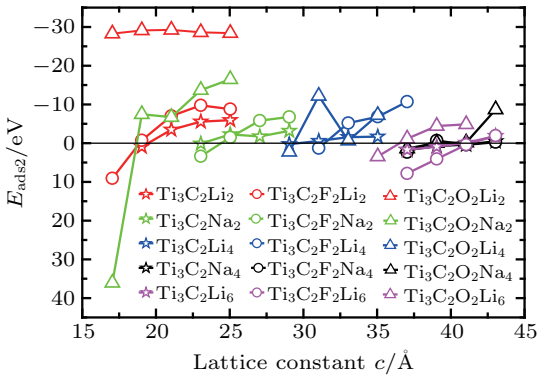


Fig. 3. Calculated E_{ads2} values of most energetically favorable structures of different intercalation layers as a function of lattice constant c.

After the thorough calculation for E_{ads2} of all the configurations, we subsequently extend our computations to their theoretical capacity, and the optimal ratio of the capacity to structure is obtained in the stacking structure. The optimum lattice constant c and the calculated capacities corresponding to different incorporation layers are listed in the following Table 2. The value of Li capacity can be increased from

251.16 mAh·g^{-1} (1280.75 mAh·cm^{-3}) to 768.68 mAh·g^{-1} (1767.61 mAh·cm^{-3}), when the c-axis value is expanded from 17.04 Å to 43.04 Å. The value of calculated C_{MNa} can be increased from 218.32 mAh·g^{-1} to 413.13 mAh·g^{-1} when the c-axis value is expanded from 19.04 Å to 43.04 Å, and the value of calculated C_{VNa} can reach 1146.18 mAh·cm^{-3} when the value of the c axis varies in the same range. The maximum value of the calculated C_{MNa} accords well with the previously reported value of 413.0 mAh·g^{-1}.[26] The difference in calculated C_{M} between Li and Na atoms with the same valence state can be attributed to their different atomic weights in the case of the same incorporation layers, thus, the heavier ions have lower gravimetric capacity. The difference in calculated C_{V} is partially due to their difference in optimal structure in the case of the same incorporation layers, thus, the large lattice volume has lower volumetric capacity. The theoretical value of the calculated capacity varies with the length of the lattice constant c, however, this change is not the process of linear increase. For example, the increased percentage of the theoretical C_{VLi} of Ti_3C_2 nanosheet slows down with each additional intercalation layer, and the theoretical C_{VNa} of $Ti_3C_2O_2$ nanosheet decreases with the lattice constant c increasing. Therefore, the proper mass load and interlayer spacing of the experimental sample are essential to obtain optimal performance of electrode material.

Table 2. Calculated optimized V_{cell} values (in unit Å^3), and calculated C_{VM} values (in units mAh·cm^{-3}) and C_{MM} values (in mAh.·g^{-1}) of $Ti_3C_2M_{2y}$ and $Ti_3C_2T_2M_{2y}$ systems.

System	y	V_{cell}	C_{VLi}	$C_{M\mathrm{Li}}$	V_{cell}	C_{VNa}	$C_{M\mathrm{Na}}$
$Ti_3C_2M_{2y}$	1	171.74	1037.26	295.42	204.39	871.57	251.03
	2	253.37	1406.16	548.86	351.32	1014.16	413.13
	3	334.99	1595.33	768.68	–	–	–
$Ti_3C_2F_2M_{2y}$	1	155.42	1146.18	244.28	204.39	871.57	213.12
	2	269.69	1321.07	459.50	351.32	1014.16	360.37
	3	351.32	1521.17	650.55	–	–	–
$Ti_3C_2O_2M_{2y}$	1	139.09	1280.75	251.16	155.42	1146.18	218.32
	2	253.37	1406.16	471.63	318.67	1118.02	367.79
	3	302.34	1767.61	666.73	–	–	–

Further structural analysis can find that the interaction between the different $Ti_3C_2T_2$ layers is ignored, when the c-axis value is expanded to more than 43.04 Å, because the layer spacing of surface terminations between two layered hexagonal structures exceeds the distance of the van der Waals interaction. In fact, the $Ti_3C_2T_x$ monolayer is difficult to prepare into the experimental samples, and sample generally belongs to a mixture of few-layer, multilayer and even bulk structure, their lattice constant c is in a range between 19.50 Å and 35.04 Å.[20,44] It is determined that two to four layers of Li atoms can be incorporated into the interlayer space of experimental samples, and one to two layers of Na atoms can be incorporated into the same interlayer space. The optimal values of theoretical capacity corresponding to experimental samples are 1406.16 mAh·cm^{-3} for calculated C_{VLi}, 548.86 mAh·g^{-1} for calculated C_{MLi}, 1146.18 mAh·cm^{-3} for calculated C_{VNa}, and 251.03 mAh·g^{-1} for calculated C_{MNa}, respectively. Although, the theoretical capacity of Na atom is much lower than that of Li atom, which is in agreement with the experimentally observed Na capacity.[32,45,46] However, the theoretical C_{Na} value is comparable to that in the case of other electrode material, such as 146 mAh·g^{-1} of MoS_2.[9] The $Ti_3C_2T_x$ nanosheets are a good candidate for being used as an electrode material in NIBs.

In experiments, bare Ti_3C_2 without any surface termination has never been achieved, thus understanding the effect of surface terminations on storage performance is particularly important.[47,48] Here, taking the $Ti_3C_2Li_{2y}$ and $Ti_3C_2T_2Li_{2y}$ as the representative cases, the influence of T-terminations on calculated value of C_{V} is analyzed. The optimum lattice constant c for incorporation one atomic layer on each surface of single layer is calculated to be 21.04 Å for Ti_3C_2, 19.04 Å for $Ti_3C_2F_2$, and 17.04 Å for $Ti_3C_2O_2$. The optimum lattice constant c for incorporation two atomic layers is calculated to be 31.04 Å for Ti_3C_2 and $Ti_3C_2O_2$, and 33.04 Å for $Ti_3C_2F_2$. The optimal lattice constant c for incorporation three atomic layers is calculated to be 41.04 Å for Ti_3C_2, 43.04 Å for $Ti_3C_2F_2$, and 37.04 Å for $Ti_3C_2O_2$. The optimized lattice parameter of $Ti_3C_2O_2Li_{2y}$ nanosheet is smaller than that of the $Ti_3C_2Li_{2y}$ nanosheet and $Ti_3C_2F_2Li_{2y}$ nanosheet. On the basis of the small lattice parameter, the $Ti_3C_2O_2Li_{2y}$ system generally possesses a small molar volume. Thus, the O-terminated Ti_3C_2 nanosheet can hold more incorporation atoms than any other nanosheets when their volumes are equal. The O functional group as an excellent chemical modifier of surfaces can greatly improve the volumetric capacity of Ti_3C_2 system. However, a process of surface functionalization with fluorine group is not responsible for increasing the volumetric capacity. The higher volumetric capacity performance can be obtained by regulating the main surface termination of sample in experimental preparation due to the effect of different surface functional groups on theoretical capacity. The above analysis of the effect

of functionalized surface on theoretical capacity is consistent with previous experimental and theoretical results.[12,17,25]

3.4. Analysis of capacity difference for the Li/Na atoms into nanosheets

It is noticed that the number of intercalation Na atom layers on each surface is only two, when the value of c-axis lattice constant varies in a range from 19.04 Å to 43.04 Å. Although, the Li/Na atoms intercalated into nanosheets have a similar operating mechanism which may be the formation of $Ti_3C_2M_{2y}$ and $Ti_3C_2T_2M_{2y}$ after intercalating M atoms into the space vacated by the Al atoms.[24] However, the intercalation layers' number of Na atom is far less than that of Li atom. We seek to understand the reason why the theoretical capacity of Na atoms is lower than that of Li atoms. Taking the twelve stable configurations of $Ti_3C_2M_{2y}$ system and $Ti_3C_2T_2M_{2y}$ system with the c-axis lattice constant of 25.04 Å ($y = 1$) and 35.04 Å ($y = 2$) for example, the formation process of M-ions' intercalation can be divided into two parts. First, the Ti_3C_2 substrate is strained to the configuration identical to that of the Li/Na-intercalated surfaces. Second, the Li/Na-ions are intercalated into the nanosheets.

In the first process, there are two kinds of energy losses that can be obtained for the substrate after deformation. First, the calculated total energy of Ti_3C_2 substrates of Ti_3C_2 nanosheet and $Ti_3C_2T_2$ nanosheet after crystal deformation has had an energy cost ($E_{ec1} = |(E_{system}$(deformation Ti_3C_2 substrates) $- E_{system}$(perfect Ti_3C_2 substrates)|), second, the calculated total energy of $Ti_3C_2T_2$ nanosheet after crystal deformation also has an energy cost ($E_{ec2} = |(E_{system}$(deformation $Ti_3C_2T_2$ nanosheets) $- E_{system}$ (perfect $Ti_3C_2T_2$ nanosheets)|)). The calculated values of E_{ec1} and E_{ec2} reveal the degree of substrates' deformation. Once the calculated value is greater than zero, the substrate produces a larger lattice deformation. The calculated E_{ec1} value of the Na atom incorporation is similar to that of the Li atom incorporation into corresponding nanosheet as shown in Fig. 4. The energy loss of Ti_3C_2 substrate is almost negligible in the Li/Na-ion insertion processes. The Ti_3C_2 substrate only shows slight structural distortion in the insertion processes, which is consistent with previous experimental result.[32] This excellent structural stability of substrate is a necessary condition for the mechanical and electrochemical stability of electrode materials. Furthermore, the calculated E_{ec2} value of the Na atom incorporation is smaller than that of the Li atom incorporation into corresponding nanosheet. Although Li-ion has a smaller ion radius than Na-ion, the functionalized substrate with Li incorporation needs to produce a larger shift of surface termination, which can adjust the substrate to adapt the ion intercalated into nanosheets. Obviously, the E_{ec1} and E_{ec2} do not embody the origin of the low Na capacity.

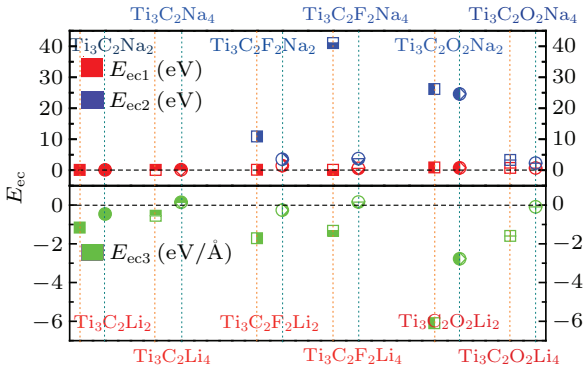


Fig. 4. Calculated E_{ec1}, E_{ec2}, and E_{ec3} values of most favorable configuration of $Ti_3C_2M_{2y}$ and $Ti_3C_2T_2M_{2y}$ nanosheet for c-axis lattice constant of 25.04 Å ($y = 1$) and 35.04 Å ($y = 2$), where y represents the number of intercalation layers on one side of single layer.

In the second process, the energy cost ($E_{ec3} = E_{ads}/h_{totave}$) is determined after the metal atoms have adsorbed on the surfaces, here, $E_{ads} = E_{adatom@system} - E_{system} - 8yE_{atom}$, with $E_{adatom@system}$ and E_{system} being the total energy of adsorbed system and unadsorbed system, E_{atom} being the energy of per metal atom from the bulk metal, y representing the number of adsorption layers on every surface of single layer, h_{totave} denoting the average vertical height from the outermost layer of metal atom to the surface layer of Ti(1) atom. The coefficient $8\times y$ represents the total number of adsorption atoms on the both sides of single layer. The calculated E_{ec3} value reveals the binding degree of substrate to metal atoms, which mainly includes the interaction of polar surfaces with cation and the electrostatic exclusion between adsorbed cation.[49] Once the calculated value is less than zero, the substrate produces the binding energy to the metal atoms. The calculated E_{ec3} values are also shown in Fig. 4, and corresponding configurations are displayed in Fig. 5. The calculated E_{ads} value of Na atom is higher than that of Li atom, and the calculated h_{totave} value of Na atom becomes larger that of Li atom, thus, the calculated E_{ec3} value exhibits a maximum value at Na-ion intercalation. Clearly, the calculated E_{ec3} values reveal that the substrate has ability to more weakly bind Na atom than Li atom. This suggests the reason why low Na capacity is related directly to the coupling strength of the Na-ion with substrate and the electrostatic exclusion between adsorbed Na-ions.

In addition, the dispersive electron cloud plays a key role in analyzing the interaction of the ions with substrate and the electrostatic exclusion between ions. The electron density difference of the (110) atomic plane among the twelve stable configurations is examined as shown in Fig. 6. For the $Ti_3C_2T_2$ substrate, the local electron transfer between the Li/Na and substrate surface is more apparent than for the Ti_3C_2 substrate. The presence of F- or O-terminations conduces to the electron transfer from the Li/Na atom to the surface. It is noticed that the interaction between the Na-ions and the substrate is weaker than that between the Li-ions and substrate. This weaker interaction can further increase the calculated value of E_{ec3}. Furthermore, the common charge quantity between the Na-ion

layers is significantly less than that between the Li-ion layers. This characteristic indicates that the electrostatic exclusion between the Na-ions layers is greater than that between the Li-ion layers. Based on the above analysis, the reason for the low Na capacity is attributed to the weak interaction between the Na atoms and the substrate and the strong electrostatic exclusion between adsorbed Na atoms. Therefore, the energy cost at zero temperature and the electron distribution can explain why the theoretical capacity of Na atoms is lower than that of Li atoms on $Ti_3C_2T_x$ nanosheet.

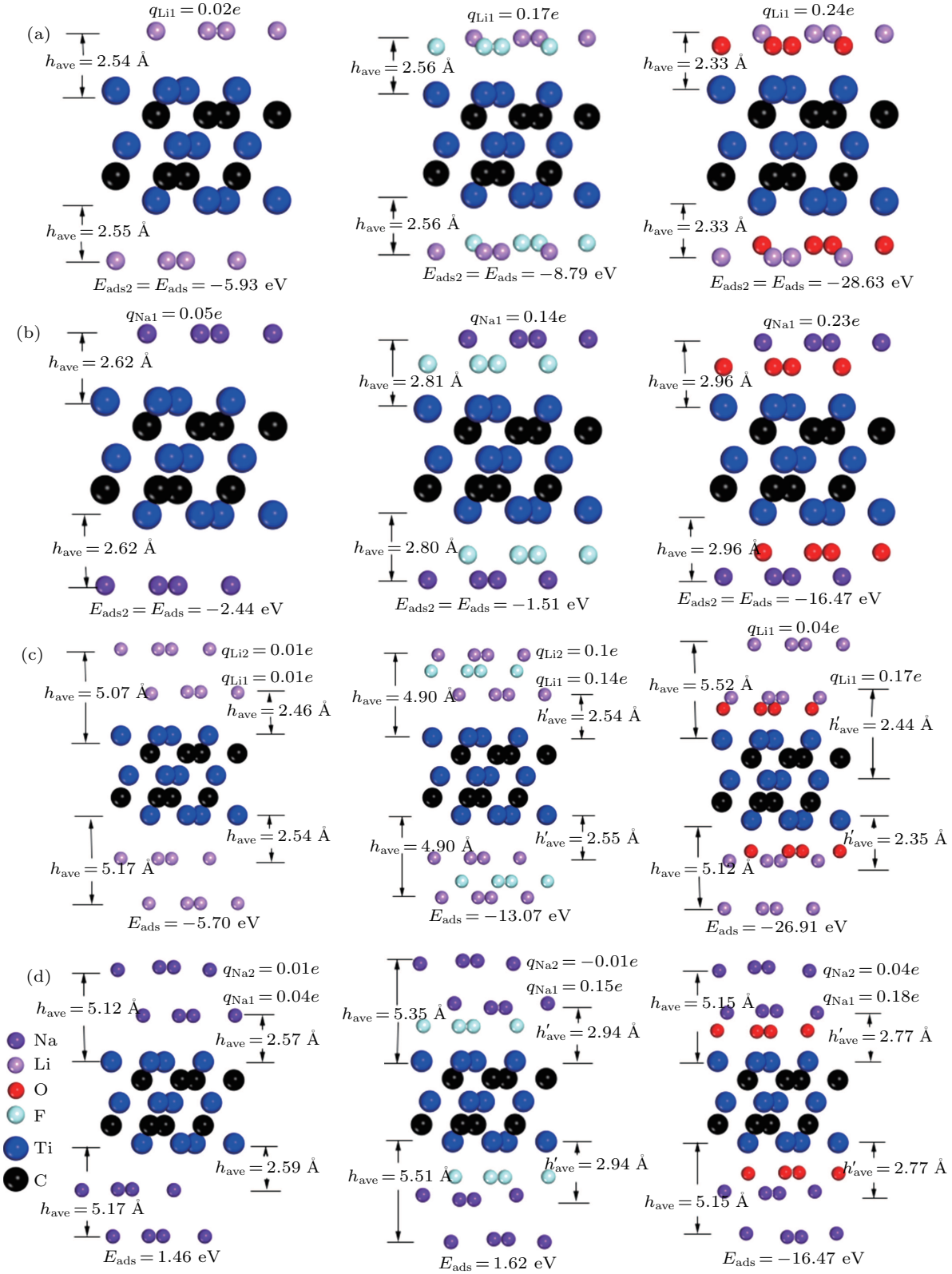


Fig. 5. Twelve stable configurations of (a) $Ti_3C_2Li_2$ and $Ti_3C_2T_2Li_2$, (b) $Ti_3C_2Na_2$ and $Ti_3C_2T_2Na_2$ systems with the c-axis lattice constant of 25.04 Å, and (c) $Ti_3C_2Li_4$ and $Ti_3C_2T_2Li_4$, (d) $Ti_3C_2Na_4$ and $Ti_3C_2T_2Na_4$ systems with the c-axis lattice constant of 35.04 Å. Note: $h_{totave} = h_{ave}$(top) $+h_{ave}$(bottom), where h_{ave}(top) and h_{ave}(bottom) are the average vertical height from the upper or lower layers of Li/Na atoms to the corresponding surface layer of Ti(1) atoms.

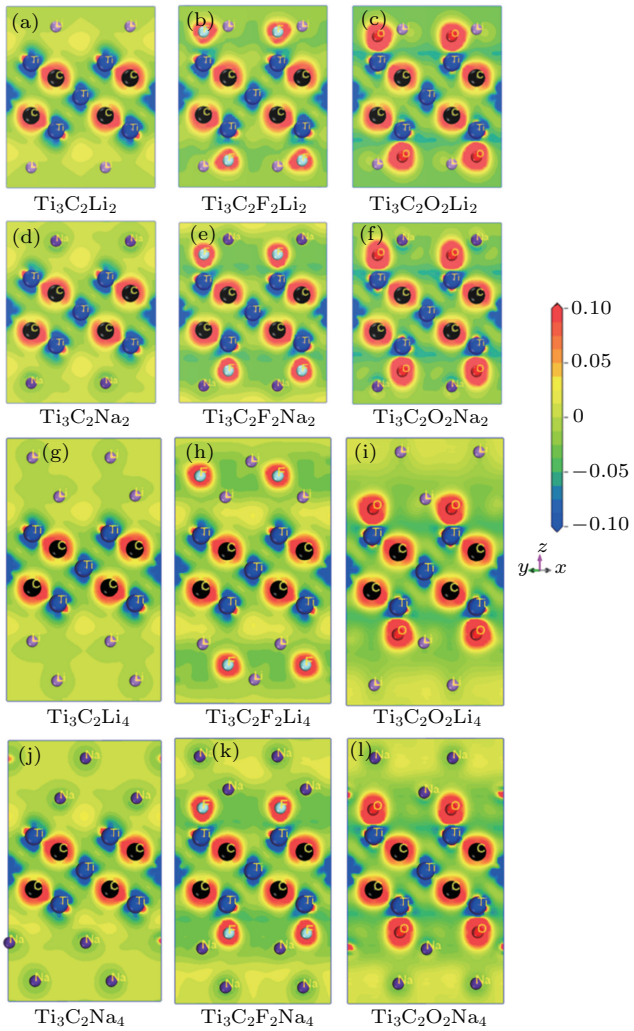


Fig. 6. Electron density difference of the (110) atomic plane among (a) $Ti_3C_2Li_2$, (b) $Ti_3C_2F_2Li_2$, (c) $Ti_3C_2O_2Li_2$, (d) $Ti_3C_2Na_2$, (e) $Ti_3C_2F_2Na_2$, (f) $Ti_3C_2O_2Na_2$ nanosheets for *c*-axis lattice constant of 25.04 Å, and among (g) $Ti_3C_2Li_4$, (h) $Ti_3C_2F_2Li_4$, (i) $Ti_3C_2O_2Li_4$, (j) $Ti_3C_2Na_4$, (k) $Ti_3C_2F_2Na_4$, (m) $Ti_3C_2O_2Na_4$ nanosheets for *c*-axis lattice constant of 35.04 Å. Blue color indicates the loss of electron density and red color indicates the enrichment of electron density compared with the sphere electron density in atoms. The color scale is in units of e·Å^{-3}.

4. Conclusions

In this work, the intrinsic structures of Ti_3C_2-based nanosheets and the corresponding theoretical capacities are investigated by first-principles calculations. The analysis of the optimal ratio of capacity to structure indicates that the increase of the interlayer spacing will be helpful in improving the capacity of MXene, which is attributed to the increase of the intercalation layers' number of *M* atoms. Meanwhile, O-terminated Ti_3C_2 surfaces improve the volumetric capacity performance of Ti_3C_2 nanosheets. The calculated C_V value can reach 1767.61 mAh·cm^{-3} based on the Li intercalation and 1146.18 mAh·cm^{-3} based on the Na intercalation. Our calculations demonstrate that the energy storage performance of MXene is tunable by using surface modification. Further, the reason for theoretical capacity differences of Li/Na atoms is analyzed, which is attributed to difference in the interaction of the *M*-ions with substrate and the electrostatic exclusion between adsorbed *M*-ions. Our findings can be useful in designing MXene-based electrode materials for energy storage applications.

Acknowledgment

The calculations were carried out by using the supercomputer resource provided by the High Performance Computing Center of Harbin Normal University and the High Performance Computing Center of Harbin Institute of Technology.

References

[1] El-Kady M F, Ihns M, Li M P, Hwang J Y, Mousavi M F, Chaney L, Lech A T and Kaner R B 2015 *Proc. Natl. Acad. Sci. USA* **112** 4233
[2] Bhimanapati G R, Lin Z and Robinson J A 2015 *ACS Nano* **9** 11509
[3] Wang G, Yang J, Park J, Gou X, Wang B, Liu H and Yao J 2008 *J. Phys. Chem. C* **112** 8192
[4] Dikin D A, Stankovich S, Zimney E J, Piner R D, Dommett G H, Evmenenko G, Nguyen S T and Ruoff R S 2007 *Nature* **448** 457
[5] Zhou X F, Fang H Y and Tang C M 2019 *Acta Phys. Sin.* **68** 053601 (in Chinese)
[6] Luan X W, Sun J P, Wang F G, Wei H L and Hu Y F 2019 *Chin. Phys. B* **28** 026802
[7] Zou F, Hu X, Li Z, Qie L, Hu C, Zeng R, Jiang Y and Huang Y 2014 *Adv. Mater.* **26** 6622
[8] Liu H, Neal A T, Zhu Z, Luo Z, Xu X, Tománek D and Ye P D 2014 *ACS Nano* **8** 4033
[9] Mortazavi M J, Wang C, Deng J K, Shenoy V B and Medhekar N V 2014 *J. Power Sources* **268** 279
[10] Naguib M, Mashtalir O, Carle J, Presser V, Lu J, Hultman L, Gogotsi Y and Barsoum M W 2012 *ACS Nano* **6** 1322
[11] Naguib M, Mochalin V N, Barsoum M W and Gogotsi Y 2014 *Adv. Mater.* **26** 992
[12] Khazaei M, Ranjbar A, Arai M, Sasaki T and Yunoki S 2017 *Nat. Rev.* **2** 16098
[13] Khazaei M, Ranjbar A, Arai M, Sasaki T and Yunoki S 2017 *J. Mater. Chem. C* **5** 2488
[14] Zhang S J, Ji W X, Zhang C W, Zhang S F, Li P, Li S S and Yan S S 2018 *Chin. Phys. Lett.* **35** 087303
[15] Wang C, Peng Q Q, Fan X W, Liang W Y, Zhang F, Liu J and Zhang H 2018 *Chin. Phys. B* **27** 094214
[16] Barsoum M W 2000 *Prog. Solid St. Chem.* **28** 201
[17] Xie Y, Naguib M, Mochalin V N, Barsoum M W, Gogotsi Y, Yu X Q, Nam K W, Yang X Q, Kolesnikov A I and Kent P R C 2014 *J. Am. Chem. Soc.* **136** 6385
[18] Hope M A, Forse A C, Griffith K J, Lukatskaya M R, Ghidiu M, Gogotsi Y and Grey C P 2016 *Phys. Chem. Chem. Phys.* **18** 5509
[19] Hong Ng V M, Huang, Zhou K, Lee P S, Que W X, Xu Z C and Kong L B 2017 *J. Mater. Chem. A* **5** 3039
[20] Naguib M, Kurtoglu M, Presser V, Lu J, Niu J J, Heon M, Hultman L, Gogotsi Y and Barsoum M W 2011 *Adv. Mater.* **23** 4248
[21] Ren C E, Hatzell K B, Alhabeb M, Ling Z, Mahmoud K A and Gogotsi Y 2015 *J. Phys. Chem. Lett.* **6** 4026
[22] Ghidiu M, Lukatskaya M R, Zhao M Q, Gogotsi Y and Barsoum M W 2014 *Nature* **516** 78
[23] Hu T, Wang J M, Zhang H, Li Z J, Hu M M and Wang X H 2015 *Phys. Chem. Chem. Phys.* **17** 9997
[24] Xie Y, Dall'Agnese Y, Naguib M, Gogotsi Y, Barsoum M W, Zhuang H L and Kent P R C 2014 *ACS Nano* **8** 9606
[25] Tang Q, Zhou Z and Shen P W 2012 *J. Am. Chem. Soc.* **134** 16909
[26] Yu Y X 2016 *J. Phys. Chem. C* **120** 5288
[27] Er D, Li J W, Naguib M, Gogotsi Y and Shenoy V B 2014 *ACS Appl. Mater. Interfaces* **6** 11173
[28] Xie Y and Kent P R C 2013 *Phys. Rev. B* **87** 235441
[29] Zhan C, Sun W W, Xie Y, Jiang D and Kent P R C 2019 *ACS Appl. Mater. Interfaces* **11** 24885
[30] Lukatskaya M R, Mashtalir O, Ren C E, Dall'Agnese Y, Rozier P, Taberna P L, Naguib M, Simon P, Barsoum M W and Gogotsi Y 2013 *Science* **34** 1502

[31] Xiong D B, Li X F, Bai Z M and Lu S G 2018 *Small* **14** 1703419
[32] Kajiyama S, Szabova L, Sodeyama K, Iinuma H, Morita R, Gotoh K, Tateyama Y, Okubo M and Yamada A 2016 *ACS Nano* **10** 3334
[33] Xie X Q, Kretschmer K, Anasori B, Sun B and Wang G X 2018 *ACS Appl. Nano Mater.* **1** 505
[34] Segall M D, Lindan P J D, Probert M J, Pickard C J, Hasnip P J, Clark S J and Payne M C 2002 *J. Phys.: Condens. Matter* **14** 2717
[35] Perdew J P, Chevary J A, Vosko S H, Jackson K A, Pederson M R, Singh D J and Fiolhais C 1992 *Phys. Rev. B* **46** 6671
[36] Grimme S J 2004 *Comput. Chem.* **25** 1463
[37] Wen J, Zhang X T and Gao H 2017 *Phys. Chem. Chem. Phys.* **19** 9509
[38] Wen J, Zhang X T and Gao H 2018 *Physica B: Condens. Matter* **537** 155
[39] Rao D W, Zhang L Y, Wang Y H, Meng Z S, Qian X Y, Liu J H, Shen X Q, Qiao G J and Lu R F 2017 *J. Phys. Chem. C* **121** 11047
[40] Weng H M, Ranjbar A, Liang Y, Song Z D, Khazaei M, Yunoki S, Arai M, Kawazoe Y, Fang Z and Dai X 2015 *Phys. Rev. B* **92** 075436
[41] Hu T, Li Z J, Hu M M, Wang J M, Hu Q M, Li Q Z, Wang X H 2017 *J. Phys. Chem. C* **121** 19254
[42] Fu Q S, Wen J, Zhang N, Wu L L, Zhang M Y, Lin S Y, Gao H and Zhang X T 2017 *RSC Adv.* **7** 11998
[43] Jin Q, Zhang N, Zhu C C, Gao H and Zhang X T 2018 *Nanoscale* **10** 16935
[44] Mashtalir O, Naguib M, Mochalin V N, DallAgnese Y, Heon M, Barsoum M W and Gogotsi Y 2013 *Nat. Commun.* **4** 1716
[45] Guo X, Xie X, Choi S, Zhao Y, Liu H, Wang C, Chang S and Wang G 2017 *J. Mater. Chem. A* **5** 12445
[46] Xie X, Zhao M Q, Anasori B, Maleski K, Ren C E, Li J, Byles B W, Pomerantseva E, Wang G and Gogotsi Y 2016 *Nano Energy* **26** 513
[47] Zhang X, Zhang Z H and Zhou Z 2018 *J. Energy Chem.* **27** 73
[48] Liu F F, Liu Y C, Zhao X D, Liu X B and Fan L Z 2019 *J. Mater. Chem. A* **7** 16712
[49] Liu Y Y, Merinov B V and Goddard A 2016 *Proc. Natl. Acad. Sci. USA* **13** 3735